UDC 615.2
DOI: 10.15587/2519-4852.2025.338156

PHARMACOLOGICAL EVALUATION AND POTENTIAL EPIGENETIC MODULATION OF A ZINC-CYSTEINE COMPLEX FOR TYPE 2 DIABETES THERAPY

Godzelle Ogoc Bulahan, Orlie B. Basalo, Hajime Iwamoto, Aaron L. Degamon, James V. Lavilla Jr., Richemae Grace R. Lebosada, Charlie A. Lavilla Jr.

Type 2 Diabetes (T2D) is a complex metabolic disorder that involves more than just glucose imbalance. Protein glycation, and epigenetic dysregulation – particularly aberrant DNA methylation – play critical roles in the onset and progression of the disease. However, current therapies remain limited in directly targeting these underlying molecular mechanisms.

The aim. *This study investigated a zinc-monocysteine complex (ZMC) as a potential multi-target therapeutic candidate for T2D, exploring its novel application in modulating protein glycation and DNA methylation events.*

Materials and methods. *The structural integrity of ZMC was confirmed through NMR, FT-IR, UV-visible, CHN analysis, and powder XRD techniques. In vitro assays compared ZMC and unbound L-cysteine (CYS) for their abilities to inhibit advanced glycation end-products (AGEs) and preserved protein secondary structure under glycation stress, using BSA-glucose and methylglyoxal (MGO) model systems. To support potential epigenetic modulation, molecular docking studies were conducted to evaluate the interaction of ZMC with DNA methyltransferase, DNMT1. Live-cell imaging was performed on C2C12 and HEK293T cells to assess changes in methylation-associated signals following ZMC treatment.*

Results. *ZMC was defined structurally as a 1:1 amorphous cyclic salt. It outperformed CYS in inhibiting AGE formation at 5 mM (BSA-glucose) and 1 mM (BSA-MGO). It also better preserved protein secondary structure at 5 mM (BSA-glucose) and 10 mM (BSA-MGO). Although docking suggested limited affinity for DNA methyltransferase (DNMT1: –5.1 kcal/mol), live-cell imaging indicated reduced methylation-associated signals in especially in C2C12 cells following treatment.*

Conclusion. *Together, ZMC demonstrates multi-target potential in addressing key metabolic and epigenetic factors involved in T2D. Its protective effects are primarily attributed to metabolic regulation. These findings support the continued development of ZMC as a promising scaffold for future T2D therapeutics*

Keywords: *type 2 Diabetes, zinc-cysteine complex, AGEs, DNA methylation, molecular docking*

How to cite:
Bulahan, G. O., Basalo, O. B., Iwamoto, H., Degamon, A. L., Lavilla, J. V. Jr., Lebosada, R. G. R., Lavilla, C. A. Jr. (2025). Pharmacological evaluation and potential epigenetic modulation of a zinc-cysteine complex for type 2 diabetes therapy. ScienceRise: Pharmaceutical Science, 4 (56), 65–77. http://doi.org/10.15587/2519-4852.2025.338156

1. Introduction

Diabetes mellitus is a major global health challenge, with Type 2 Diabetes (T2D) accounting for approximately 90% of all cases [1, 2]. The International Diabetes Federation (IDF) estimates 537 million individuals are living with diabetes in developed regions [1], while The Lancet reports over 800 million globally, a fourfold increase since 1990, with prevalence doubling from 7% to 14% by 2022 [3]. In the Philippines, 2021 data reported 4.3 million diagnosed and 2.8 million undiagnosed cases [4].

Persistent hyperglycemia promotes the formation of advanced glycation end-products (AGEs) through non-enzymatic glycation of proteins, lipids, and nucleic acids [5, 6]. AGEs impair biomolecular functions, contribute to diabetic complications, and activate receptors that exacerbate oxidative stress [6, 7].

In addition to genetic predisposition, modifiable factors such as aging, obesity, and physical inactivity influence DNA methylation (DNam) patterns in tissues including pancreatic islets, adipose, and skeletal muscle [8–10]. Epigenetic dysregulation has emerged as a critical mechanism in T2D pathophysiology.

While metformin remains the standard first-line therapy due to its efficacy in lowering glycated hemoglobin (A1C), reducing weight, and improving cardiovascular outcomes [11], its limitations, including the risk of lactic acidosis, highlight the need for alternative interventions. Among emerging approaches, metal-based therapeutics, particularly zinc (Zn) complexes, have shown promise due to Zn's insulin-mimetic and antioxidant properties [12]. Zn complexation with amino acids or peptides has been shown to enhance its bioavailability and physiological effects. Notably, Zn complexes with L-carnosine [13] and L-cysteine [14] have demonstrated such benefits, with the Zn-L-carnosine complex being an approved anti-ulcer agent.

This study investigates the zinc-monocysteine complex (ZMC), a previously unexplored compound, for its potential to address key pathological features of T2D. *In silico* molecular docking and *in vitro* analyses were conducted to evaluate its effects on glucose- and methylglyoxal (MGO)-induced protein glycation, protein structural changes, and DNAm alterations. With combined properties, Zn and L-cysteine (CYS), ZMC presents a potential therapeutic candidate with a promising therapeutic role in T2D. Preliminary pharmacological profiling supports it potential for further development in T2D management.

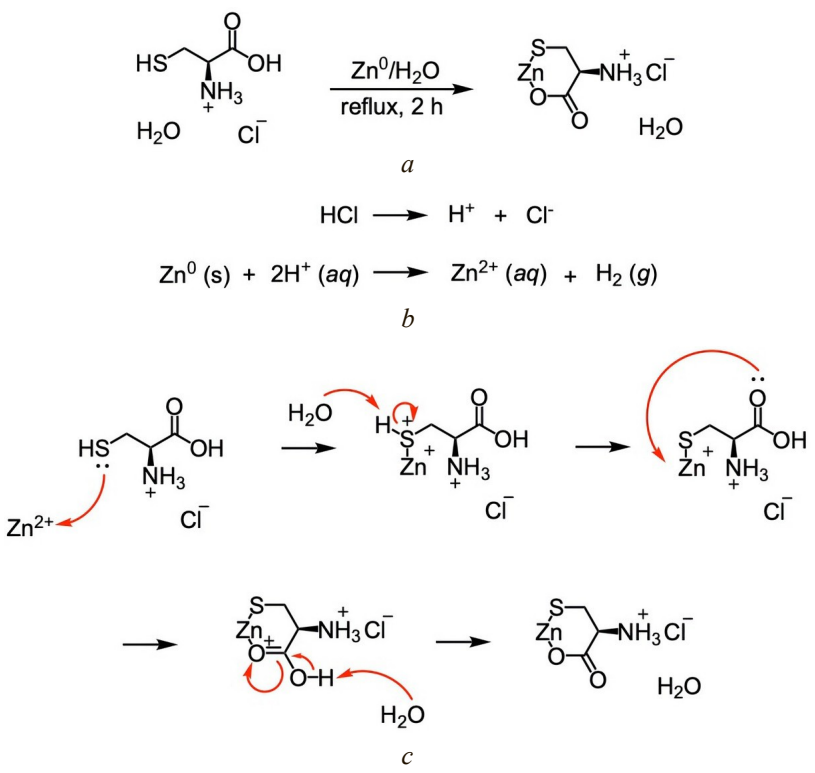

Fig. 1. Zinc-monocysteine complexation under acidic aqueous conditions: *a* – synthesis zinc-monocysteine complex under acidic aqueous conditions; *b* – ionization of elemental zinc in acidic medium: under pH ~2, provided by the dissociated HCl from L-cysteine $HCl \cdot H_2O$, Zn^0 undergoes proton-driven oxidation to Zn^{2+} with the concurrent evolution of H_2 gas. This reaction initiates the metal-ligand coordination cascade with cysteine; *c* – proposed reaction mechanism for the formation of zinc-monocysteine complex

2. Planning (methodology) of research

The methodology comprises the following experiments designed to characterize and evaluate the biological activity of ZMC:

1. Synthesize ZMC and confirm its structural integrity using NMR, FT-IR, UV-Visible spectroscopy, elemental analysis (CHN), and Powder X-ray Diffraction (PXRD).

2. Investigate the inhibitory effect of ZMC on AGE formation and its ability to preserve protein secondary structure using BSA-glucose and MGO model systems.

3. Evaluate the binding interactions of ZMC with DNA methyltransferase (DNMT1) via molecular docking approach.

4. Examine the modulatory effect of ZMC on DNAm in C2C12 and HEK293T cells using a fluorogenic synthetic molecule/protein hybrid probe.

3. Materials and methods

3. 1. Synthesis and instrumentation

The synthesis of ZMC, illustrated in Fig. 1, was performed according to the published protocol by Tate and Newsome [15], with minor modifications. A CYS (10 g) solution was prepared by dissolving it in 200 mL water, maintaining a 100 mmol concentration. Zn powder (26 g) was added at a molar ratio 0.3:2 (CYS:Zn). At room temperature, the solution was mixed for 30 min, followed by reflux at 85°C for 2 h with continuous stirring. Filtration discarded the solid residue, and a dry ice-acetone bath froze the filtrate. Lyophilization of the frozen solution yielded a dehydrated white powder. NMR spectroscopy (700 MHz Bruker AvanceNeo), UV-visible absorption (JASCO V-730 spectrophotometer), IR absorption (JASCO FT/IR-4600 spectrometer), powder x-ray diffraction (Bruker D2 Phaser 2nd Generation), and elemental analysis (CHN Analyzer Micro Cord ER JM10) confirmed the formation of the product.

3. 2. Congo red binding assay

A dye-based binding test was carried to establish whether ZMC could potentially suppress *β*-amyloid cross-structure development in BSA. The assay was performed according to the published experimental conditions outlined Miroliaei et al. [16]. Briefly, four groups of solutions: non-glycated (NG) [BSA only], glycated (GLY) [BSA (10 mg/mL) and D-glucose (90 mg/mL), and GLY in the presence of ZMC (10 mM, 5 mM, and 1 mM) and 10 mM aminoguanidine (AG). Each solution was dissolved in 3.0 mM sodium-azide containing 0.2 M phosphate-buffered saline (PBS, pH 7.4). The final volume was 1.8 mL for incubation. For 24 h, glycated groups were incubated at 60°C to speed up the reaction. On the other hand, the NG was subjected to incubation at room temperature. Subsequent to incubation, half of the test samples were added to 0.5 mL of 75-μM Congo red solution in 10% (v/v) PBS-ethanol. The remaining half was then used for background correction. The absorbance measurements were obtained via a CLARIOstar® plus multimode microplate reader (BMG Labtech, Germany) at λ_{max} of 530 nm. Moreover, an identical experiment was conducted with 60 mM MGO instead of glucose.

3. 3. AGE inhibition assays

In this assay, the inhibitory effect of the complex as an anti-sequestering agent against AGE formation was determined. The published protocol outlined by [17] was the basis for the reaction model systems with minimal alterations.

BSA-glucose model system.

Solutions of 10 mg/mL BSA and 90 mg/mL glucose were prepared separately using PBS (pH 7.4). Subsequently, the BSA-glucose mixture solution was allowed to react in the presence or absence of ZMC (10 mM, 5 mM, and 1 mM). The NG BSA solution served as the control in the experiment. Additionally, 300 μL of NaN_3 was incorporated into each test solution prior to a 7-day incubation at 37°C. The fluorescence intensity was then recorded using a CLARIOstar® plus multimode microplate reader (BMG Labtech, Germany) at 360 nm ($\lambda_{excitation}$) and 420 nm ($\lambda_{emission}$). Employing AG as the standard, the percent inhibition of AGE formation of the test samples was expressed in terms of change relative to NG control.

BSA-MGO model system.

The BSA-MGO model system was prepared first by independently dissolving 2 mg/mL BSA and 400 mg/mL MGO in PBS (pH 7.4). The succeeding steps of the protocol was identical to the BSA-glucose model, except that the incubation time was 5 days in the same dark environment at a constant temperature of 37°C. The AGE fluorescence measurement was done at 340 nm ($\lambda_{excitation}$) and 420 nm ($\lambda_{emission}$). Also, inhibition of AGE formation of the test samples was expressed in terms of change relative to NG control.

3. 4. Molecular docking study

Target protein and ligand preparation.

The three-dimensional crystal structure of human DNA methyltransferase (DNMT), DNMT1 (PDB: 4wxx), was retrieved from RCSB Protein Data Bank and rendered in UCSF Chimera v1.18. The protein structure was prepared as a PDBQT file using MGL Tools. ZMC and standard 5-aza-2'-deoxycitidine (AzadC) SMILES, were converted into a SYBYL mol2 file using Avogadro, followed by torsion analysis and PDBQT rendering with MGL Tools.

Molecular docking simulation.

Molecular docking was performed using AutodockVina v1.5.7 with a united-atom scoring function, utilizing the Perl search string command for high throughput screening. The DNMT1 crystal structure was prepared by removing existing co-crystallized ligands and water molecules. Ligand and protein structure was minimized, adding missing hydrogen atoms and assigning charges using the Gasteiger method (pH 7.40) via Amber's Antechamber module. Docking followed a "flexible ligand into flexible active site" protocol, allowing ligand flexibility and torsion within a grid box covering the enzyme's binding cavity. The model with the best affinity was selected for post-dock analysis. Protein-ligand interactions and residues were visualized using PyMOL v3.1.3.1, LigPlot+ v2.2.9, and BIOVIA Discovery Studio. The RMSD value between the co-crystallized and re-docked ligand for the protein complex was below 2 Å (1.176 Å), indicating that the docking protocol reliably reproduced the experimental binding poses and that the predicted ligand-protein conformations are accurate.

3. 5. Live-Cell imaging of methylated DNA

To visualize epigenetically modified DNA in C2C12 and HEK293T cells treated with or without ZMC, a live-cell imaging approach was employed using a hybrid fluorogenic probe system [18].

Cell culture work.

HEK293T and C2C12 cells were cultured in Dulbecco's Modified Eagle Medium (DMEM (+)) with penicillin-streptomycin (PET). After incubation, the culture medium was aspirated, and the cells were washed three times with 2 mL of PBS (washing was not required for HEK293T cells). Subsequently, 1 mL of PET was added to each dish, with an additional 1 mL of PBS for HEK293T cells. The dishes were incubated in a CO_2 incubator for 3 min. Following incubation, 2 mL of DMEM (–) was added, and the cells were gently pipetted to facilitate detachment. The cell suspension was collected into a 15 mL tube and centrifuged at 1000 rpm for 3 min, and the supernatant was aspirated. A 4 mL of DMEM (–) was added to the tube, and the suspension was thoroughly homogenized. A 20 μL aliquot of the 36 cell suspension was loaded onto an Invitrogen cytometer slide and quantified using the cell counter, with the "20-field" option selected to ensure accurate cell counting.

Transfection and confocal microscopy workflow for cultured cells.

Transfection was performed by preparing two solutions: one containing 14.55 μL OPTI-MEM mixed with 0.45 μL Lipofectamine 3000, and another containing 12.61 μL OPTI-MEM, 0.55 μL Plus reagent, and 0.592 μL HA-PYP3R-MBD_{1-112} plasmid. The first solution (13.75 μL) was combined with the second to a final volume of 27.5 μL, which was added to the cells and incubated for 24 h. For pre-imaging, culture medium was aspirated, wells washed once with 100 μL Hank's Balanced Salt Solution (HBSS), then incubated with 1 mL serum-free DMEM (pH 7.4) containing 1 μL of 2 mM PYP-ligand-conjugated Oxazole Yellow (YOCNB) at 25°C for 1 h. After aspirating, wells were washed three times with 100 μL HBSS and supplemented with 100 μL DMEM plus 10% FBS. Cell viability and adherence were confirmed prior to imaging. Confocal microscopy was performed using a Zeiss LSM 880 with a Plan Apochromat 63x/1.4 oil objective, exciting at 463 nm and detecting emission at 551 nm; images were analyzed using Zeiss LabScope software.

3. 6. Statistical analysis

The experimental assays were performed in three independent trials, each performed in triplicate. Results are expressed as ± standard error of the mean ($n \geq 3$). Where necessary, parameters were compared using ANOVA followed by Dunnett's post-hoc test, with statistical significance that was determined using an alpha value of 5% ($\alpha = 0.05$). A p-value of < 0.05 was considered statistically significant. Data analysis was carried using a GraphPad Prism v10.2.3 (394).

4. Results

4. 1. ^{1}H, ^{13}C NMR, and HSQC spectral analyses

Fig. 2, *a*, *b* present the recorded ^{1}H and ^{13}C NMR spectra of the synthesized compound, respectively, which demonstrate its high purity. In comparison to the free CYS spectra provided in Fig. 2, *d*, downfield shifts of the peaks were observed, indicating the formation of a cyclic Zn salt

with CYS [19]. As reported by Tate and Newsome, the slightly lower chemical shift for the CH_2 group in the salt form, compared to that of the free acid, suggests the binding of Zn to CYS [15]. A distinct splitting of the CH_2 group indicates that the cyclic salt is rigid, resulting in non-equivalence of the two protons in the CH_2 group. This is further confirmed by the HSQC spectrum in Fig. 2, *c*, which provides crucial information regarding the molecular connectivity, specifically the correlation between the carbon and proton atoms within the complex.

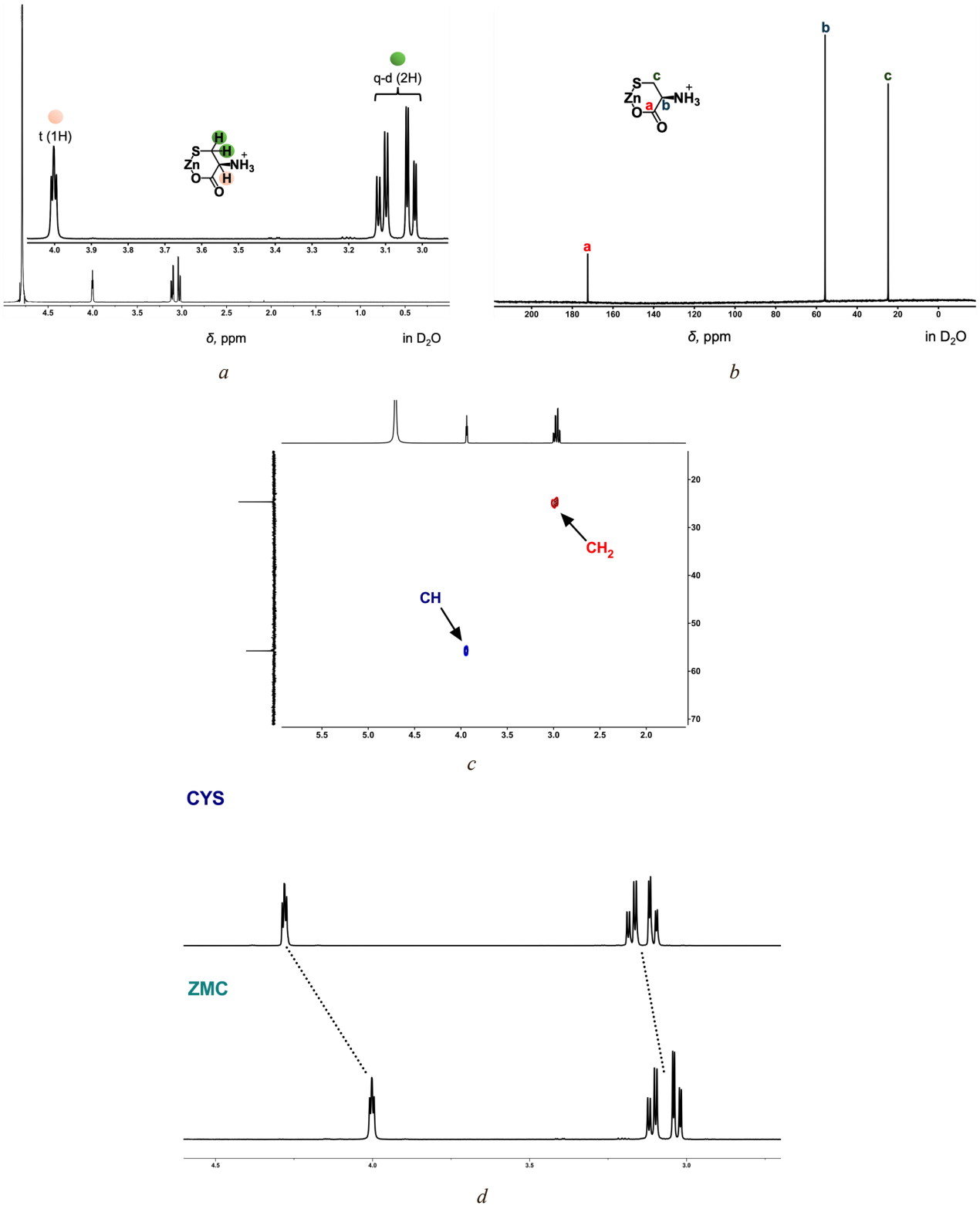

Fig. 2. NMR spectral analysis of zinc-monocysteine complex (ZMC): *a* – ^{1}H NMR spectra of ZMC cyclic hydrochloride: ^{1}H NMR (700 MHz, D_2O) δ 4.00 (t, J = 5.7 Hz, 1H), 3.15 – 2.97 (q-d, 2H) ppm; *b* – ^{13}C NMR spectra of ZMC: ^{13}C NMR (176 MHz, D_2O) δ 172.42 (C=O), 55.76 (CH), 24.74 (CH_2) ppm; *c* – HSQC spectra of ZMC: ^{13}C NMR (176 MHz, D_2O) δ 55.76, 25.05, 24.74; ^{1}H NMR (700 MHz, D_2O) δ 4.00, 3.15, 2.97; *d* – Comparative ^{1}H NMR spectral analysis of ZMC and L-cysteine (stacked mode)

4. 2. FT-IR spectral analysis

The complexation of Zn with CYS molecule was studied using FT-IR spectroscopy in ATR, with spectra of both ZMC and the free CYS shown in Fig. 3. The CYS spectrum exhibits typical bands: a large broad band between 3500–3000 cm^{-1} (A) which corresponds to the NH_3^+ asymmetric stretch and a weak narrow signal attributed to thiol (-SH) group is observed at 2611 cm^{-1} (B). The asymmetric and symmetric C=O stretching modes of the carboxylate ($-COO^-$) are observed at 1741 and 1520 cm^{-1} (C), respectively, while the less intense peaks at 1628 and 1573 cm^{-1} (C) belongs to the asymmetric and symmetric bending of NH_3^+ [20]. In the ZMC spectrum, the -SH band is absent, confirming the Zn-S bond formation [21]. The signal at 2569 cm^{-1} (E) indicates NH_3^+ stretching, not the thiol group [20]. Additionally, the carbonyl stretch 1741 cm^{-1} is less intense in ZMC, indicating that Zn binding via the thiol and carboxylate groups induced the reduction of electron density on the C=O, weakening the bond [22]. This could explain the decrease in IR intensity. The presence of broader O-H stretching band and the O-H bending band at 1622 cm^{-1} (F) suggests the presence of solvate water in the complex. This broad O-H stretch indicates that the water molecule is likely hydrogen-bonded to the complex, possibly interacting with the CYS or Zn [23]. However, the fully amorphous nature of ZMC may have also contributed to the broadening of the bands. Slight shifts in other vibrational frequencies in ZMC may be attributed to changes in charge distribution, as CYS bind to Zn, which has low electronegativity [24]. Furthermore, a series of sawtooth peaks (stretching vibrations of C-N and C-C) between 1480–1090 cm^{-1}(D) suggests the possible formation of a ring structure [25]. Table 1 presents the key FTIR spectral features that distinguish free CYS from ZMC, highlighting shifts associated with metal-ligand coordination.

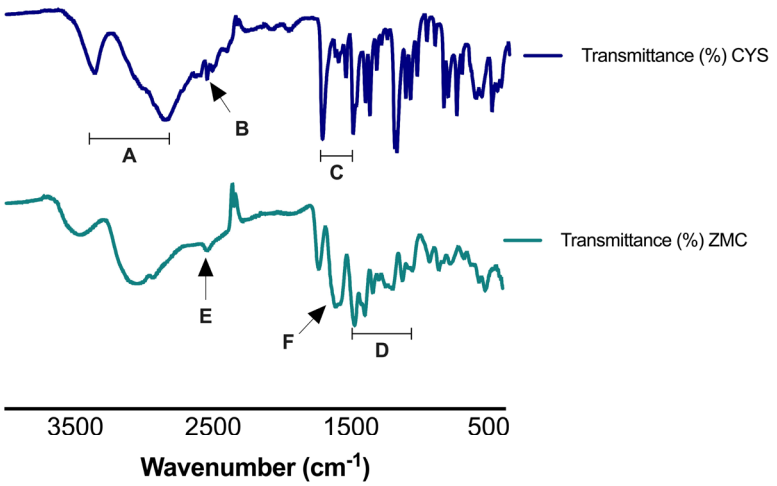

Fig. 3. FT-IR spectra of ZMC and free CYS ligand

Table 1

Comparison of key FT-IR spectral features between free cysteine and zinc-monocysteine complex

Vibrational mode	Functional group assignment	CYS (cm^{-1})	ZMC (cm^{-1})	Change upon complexation	Interpretation
N–H asymmetric stretching	NH_3^+ group	3000–3500 (broad, intense)	3000–3500 (broad, weaker)	Reduced intensity	Indicates altered hydrogen bonding, possibly due to solvate water or metal interaction
S–H stretching	Thiol (–SH) group	2611	Absent	Disappearance of –SH peak	Confirms Zn–S bond formation
N–H stretching (shoulder/overtone)	NH_3^+ overtone or interaction band	—	2569	New weak band appears	May indicate NH_3^+–Zn interaction or overtone shift
C=O asymmetric stretching	Carboxylate ($–COO^-$)	1741	Strongly diminished	Substantial reduction in peak intensity	Suggests coordination of Zn to carboxylate oxygen
C=O symmetric stretching	$–COO^-$ group	1520	Altered / shifted	Slight spectral changes	Reflects electron redistribution at carboxylate site
NH_3^+ bending	NH_3^+ group	1628, 1573	1622	Small shift and band merging	Possible interaction with water molecules or Zn center
O–H stretching & bending	Hydrogen-bonded water	Not observed	3000–3500 (broad), 1622	New broad bands appear	Indicates presence of solvate water in the complex
C–N / C–C stretching	Aliphatic backbone / cyclic features	1480–1090	1480–1090 (sawtooth peaks)	Sawtooth pattern becomes prominent	Suggests ring formation, supporting cyclic Zn–CYS complex

4. 3. UV-Visible spectral analysis

The coordination of metal ions to ligands induced a reorganization of the metal's d-orbital electronic configuration, which alters its overall electronic structure [26]. For transition metal ions that exhibit electronic absorption in the visible spectrum, ligand coordination causes shifts in the electronic configuration, resulting to observable changes. These color variations can, therefore, serve as an effective means to identify the coordination environment of the metal ion [27]. In the case of ZMC, no color change was observed upon complexation due to its

d^{10} configuration, which prevents d-d transitions, resulting in the absence of absorption bands above 400 nm. Consequently, ZMC is expected to be diamagnetic. The observed results are consistent with the reported UV data for Zn complexes of L-glutamic acid and L-aspartic acid [28]. While UV-visible spectroscopy is not ideal to detect the complexation of Zn with CYS, the minimal bathochromic shift (or red shift) in its absorption maxima indicates that the electronic environment of CYS was altered upon interaction with Zn, as depicted in Fig. 4. This can also be associated with the formation of a more stable complex [29].

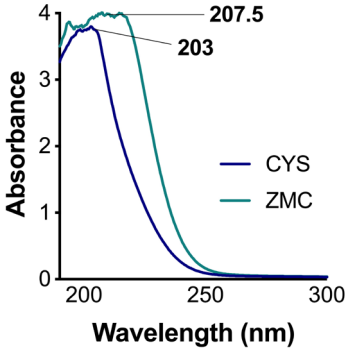

Fig. 4. UV-visible spectra of ZMC and CYS with corresponding λ_{max} (nm) values

4. 5. Elemental analysis

CHN analysis confirms the percentage composition of carbon, hydrogen, and nitrogen in our synthesized complex. The theoretical percentages of carbon, hydrogen, and nitrogen were calculated based on the established molecular formula of ZMC, as reported by Tate and Newsome, and were subsequently compared to the values obtained from elemental analysis. Minor discrepancies (within ±0.4%) likely result from trace impurities. The analysis indicates that ZMC (cyclic salt) consists of one molecule Zn and one molecule of CYS, as shown in Fig. 2 above. Moreover, elemental analysis confirms the presence of one molecule of solvate water, likely due to the compound's hygroscopic nature, which results in moisture uptake during analysis. This is corroborated by the IR spectrum, which supports the presence of water but does not suggest its integration into the core structure of the expected complex. The elemental data for ZMC is presented in Table 2.

Table 2

C, H, and N analysis of zinc-monocysteine complex

Complex	Mol. formula (Hill System)	Mol. wt. (g/mol)	Color	Elemental analysis Observed (theoretical)		
				%C	%H	%N
ZMC	$C_3H_8ClNO_3SZn$	238.99	white	14.68 (15.08)	3.49 (3.37)	5.66 (5.86)

4. 6. Powder XRD analysis

The phase of the lyophilized ZMC was determined by powder x-ray diffraction (PXRD), which revealed no detectable diffraction features as shown in Fig. 5. PXRD patterns lacked distinct Bragg peaks, confirming its completely amorphous nature. This finding agrees with the FT-IR spectrum, where the amorphous complex exhibited broadened bands, similar to the behavior observed in amorphous urea ices compared to their crystalline counterparts [30]. A synthesis of zero-valent iron nanoparticles has also been reported, with the absence of characteristic peaks, indicating that the material is amorphous [31]. Structural changes from the complexation reaction and synthesis conditions likely disrupted the crystalline structure of CYS, leading to its amorphization [32].

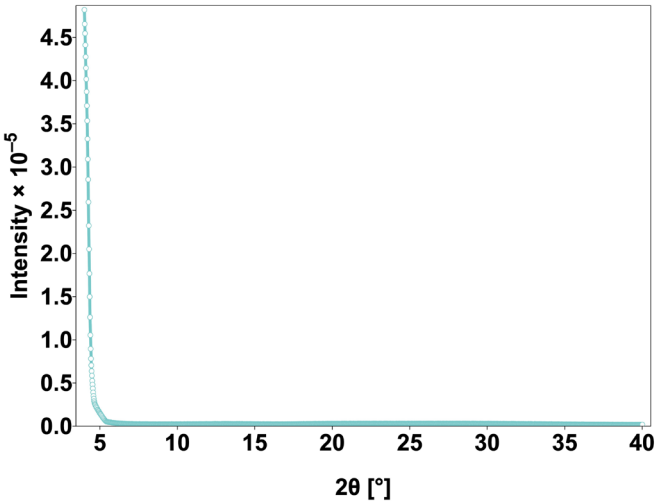

Fig. 5. Powder x-ray diffraction pattern of the synthesized ZMC. The absence of characteristic peaks indicates the amorphous nature of the complex

4. 7. ZMC Protects BSA from glycation-induced damage

Congo red assay was employed to evaluate ZMC's ability to inhibit β-sheet aggregation in BSA glycation models. As expected, the GLY showed the highest Congo red absorbance, indicative of pronounced β-sheet formation. Treatment with ZMC at concentrations 1, 5, and 10 mM significantly reduced absorbance, with 5 mM and 10 mM showing inhibition levels comparable to AG, relative to native NG BSA controls, in both BSA-glucose and BSA-MGO model systems, as shown in Fig. 6.

4. 8. ZMC effectively inhibits glycation in BSA-based models

ZMC significantly inhibited AGE formation in both BSA-glucose and BSA-MGO models, as shown in Fig. 7. In glucose-induced glycation, GLY showed a 2.71-fold increase in AGE fluorescence relative to NG. ZMC treatment at 10 and 5 mM significantly reduced AGE levels, with the most pronounced effect at 5 mM ($p < 0.0001$), surpassing AG, while 1 mM showed no significant inhibition. In the MGO model, 1 mM ZMC significantly ($p < 0.05$) reduced AGE formation, though difference from CYS was not statistically significant, despite a downward trend. When comparing 5 mM and 1 mM complex concentrations in the glucose and MGO model, respectively, ZMC demonstrated superior antiglycation activity over CYS.

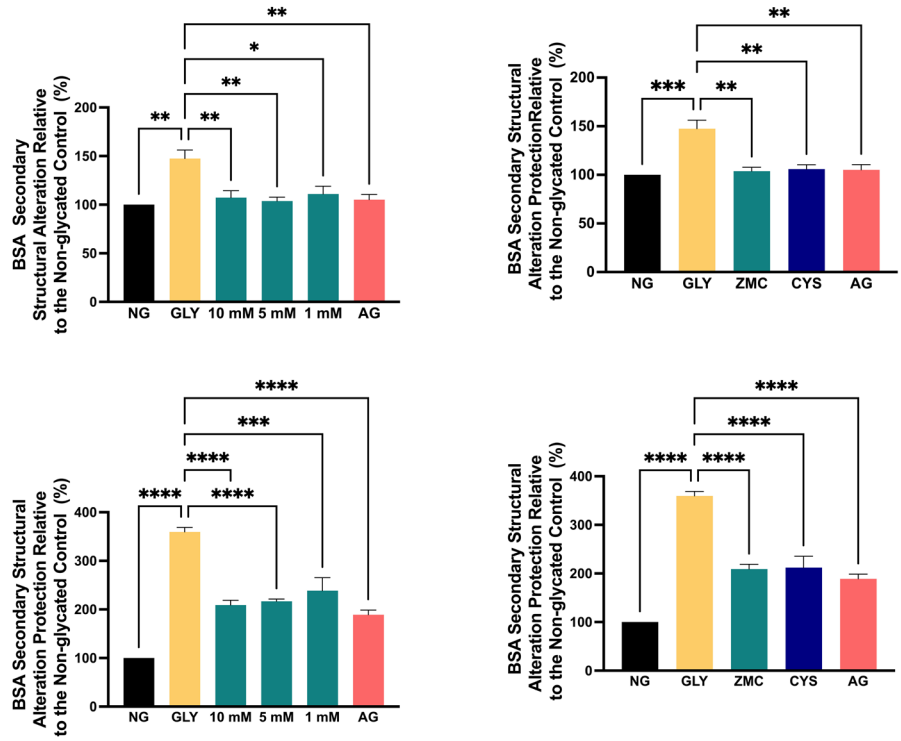

Fig. 6. Effects of ZMC treatment on glucose- and MGO-induced BSA secondary structural changes, compared to the glycated (GLY) control and standard treatment, aminoguanidine (AG): *upper panels*: BSA-glucose model; *lower panels*: BSA-MGO model. Data are presented as mean ± SEM from three independent experiments ($n = 3$), each performed in triplicate (technical replicates averaged for each experiment). Statistical analysis was performed using ordinary one-way ANOVA followed by Dunnett's multiple comparison post hoc test. Significance indicates differences relative to the GLY control: *$p < 0.05$, **$p < 0.01$, ***$p < 0.001$, and ****$p < 0.0001$

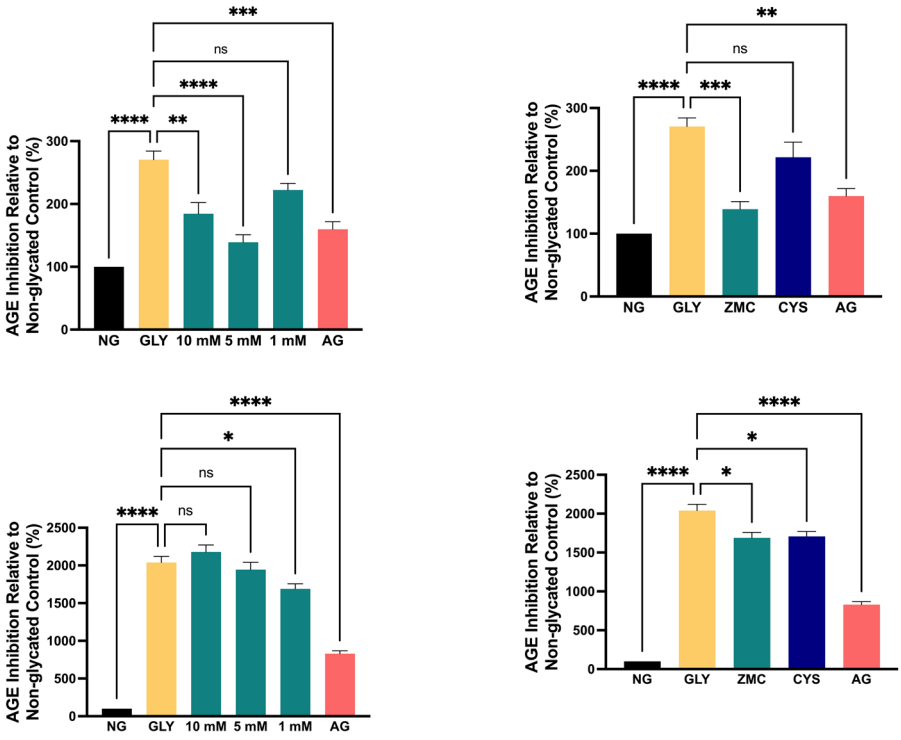

Fig. 7. ZMC effectively sequesters glucose and MGO, in comparison to the glycated (GLY) control and the standard treatment, aminoguanidine (AG): *upper panels*: BSA-glucose model; *lower panels*: BSA-MGO model. Data are presented as mean ± SEM from three independent experiments ($n = 3$), each performed in triplicate (technical replicates averaged for each experiment). Statistical analysis was performed using ordinary one-way ANOVA followed by Dunnett's multiple comparison post hoc test. Significance indicates differences relative to the GLY control: *$p < 0.05$, **$p < 0.01$, ***$p < 0.001$, and ****$p < 0.0001$

4. 9. Molecular docking of protein target analysis

Molecular docking simulations were conducted using AutoDock Vina to assess the binding interaction of ZMC with human DNMT1 (PDB: 4wxx). AzadC, a known DNMT inhibitor, served as the positive control. The ligand formed hydrogen bonds with the target protein, as illustrated in the 3D and 2D binding interaction models shown in Fig. 8, 9, respectively. The ligand generated 10 docking conformations per receptor, with a maximum of 5 hydrogen bonds per complex. ZMC exhibited Gibbs free energy (ΔG) binding affinity of –5.1 kcal/mol for DNMT1, as shown in Fig. 8, *a*. In comparison, AzadC demonstrated stronger binding with ΔG value of –6.8 kcal/mol for the same receptor, as shown in Fig. 8, *b*. These more negative ΔG values indicate stronger ligand-receptor binding, as lower ΔG correlates with higher binding affinity [33].

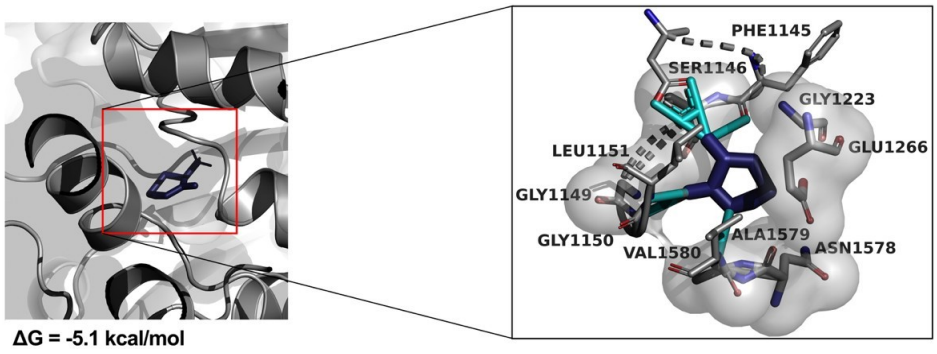

a

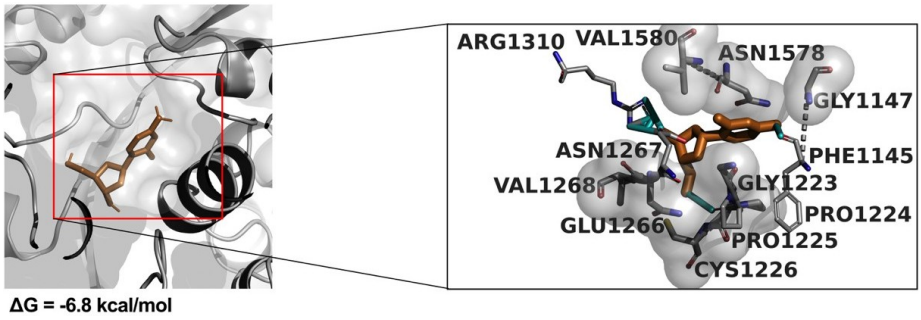

b

Fig. 8. Three-dimensional presentation of the binding interactions between ligands and protein receptors with their respective Gibbs free energy:
a – ZMC and DNMT1: 4wxx; *b* – AzadC and DNMT1: 4wxx

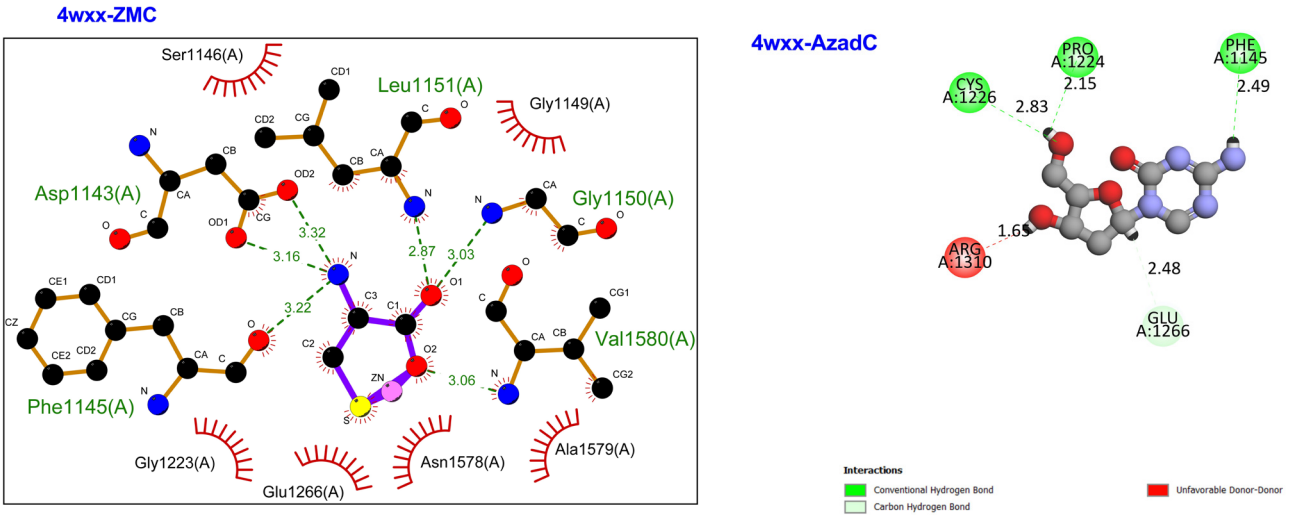

a *b*

Fig. 9. Two-dimensional interactions between protein receptors and binding ligands:
a – ZMC and DNMT1: 4wxx; *b* – AzadC and DNMT1: 4wxx

4. 10. Methylated DNA imaging in living cells

To explore the potential effects of ZMC in DNAm modulation, a fluorogenic synthetic molecule/protein hybrid probe was employed for live-cell imaging. In C2C12 cells, ZMC treatment visually reduced fluorescence intensity, with signal levels appearing similar to those of AzadC, as shown in Fig. 10. In contrast, CYS lead to a clear increase in fluorescence. In HEK293T cells, AzadC again eliminated fluorescence, confirming its strong inhibitory effect. ZMC displayed a visually lower signal than CYS, suggesting a potential inhibitory effect on DNMTs. However, these observations are based solely on visual inspection, and quantitative analyses are needed to confirm differences in methylation levels.

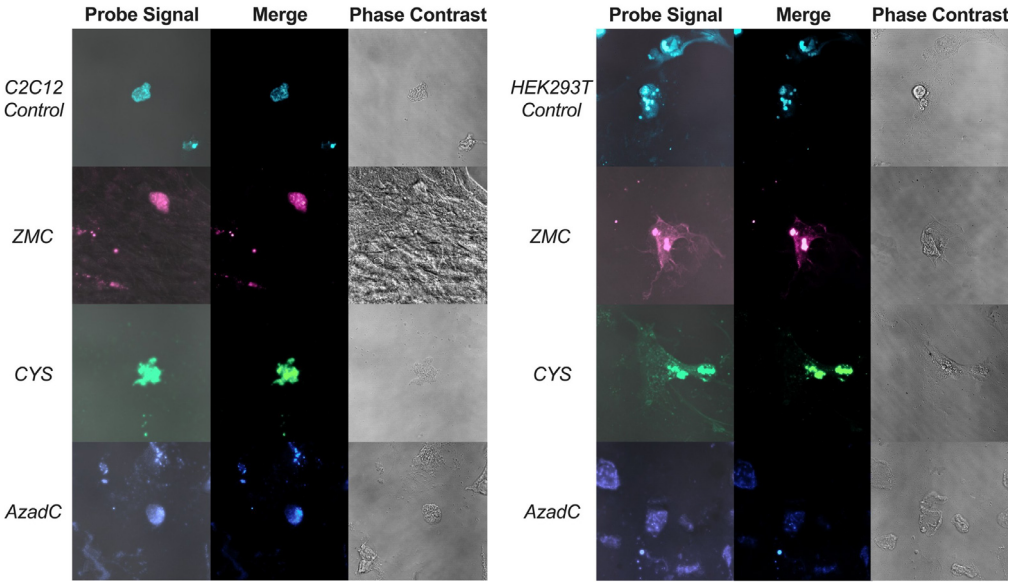

Fig. 10. Live-cell imaging of methylated DNA (Scale bar: 20 μm): *a* – effects of ZMC (30 μM), CYS (10 mM), and AzadC (25 μM) on fluorescence in nuclei. PYP3R-MBD$_{1\text{-}112}$-expressing C2C12 cells were pretreated in the presence of the tested compounds except for the control; *b* – effects of ZMC, CYS, and AzadC on fluorescence in nuclei. Identical experimental conditions were applied, except that HEK293T cells were used instead of C2C12 cells

5. Discussion

The complex pathophysiology of T2D required multifaceted therapeutic strategies that extend beyond glycemic control. To the authors' knowledge, this study is the first to evaluate the therapeutic potential of ZM, a zinc-cysteine complex, as a promising multi-target agent capable of mitigating protein glycation, modulating epigenetic dysregulation, and potentially alleviating oxidative stress in T2D.

The zinc-cysteine complex studied here demonstrates characteristic consistent with stable metal-ligand coordination, involving bidentate binding through thiol and carboxylate groups. This coordination likely contributes to its bioactivity, reflecting mechanisms seen in natural metalloproteins where zinc plays a crucial structural and catalytic role [20, 21]. The presence of hydrogen-bonded water molecules in the complex may further enhance its stability and biological interactions [23]. Changes in the electronic environment due to zinc coordination may influence the compound's function as well [28, 29].

While CYS possesses inherent antiglycation properties [34], its combination with zinc appears to enhance biological activity. Zinc is known for its antioxidative, anti-apoptotic, and redox-modulating effects, which contribute to cellular stability and protection against glycation-induced damage [35–37]. The superior performance of ZMC compared to CYS alone may be attributed to this additive synergy. Similar improvements have been reported in other zinc-based conjugates, such as carnosine-zinc complexes, which outperform AG in antiglycation assays [38]. The synergistic interaction between zinc and CYS in ZMC resembles natural zinc-cysteine coordination found in metalloproteins, which are essential for enzymatic catalysis and structural integrity [39, 40].

Molecular docking studies demonstrated that ZMC exhibits moderate affinity toward DNA methyltransferase DNMT1, forming multiple hydrogen bonds at their binding sites [41]. Although its binding energy was lower than that of the reference compound AzadC, the observed molecular interactions suggest potential for further structural optimization to enhance epigenetic modulation. Zinc acts as a structural cofactor in chromatin-associated zinc-finger proteins and DNMTs, influencing gene regulation and methylation patterns [42]. Disruption in zinc homeostasis have been linked to both global hypomethylation and gene-specific hypermethylation, which are associated with insulin resistance and diabetic complications [43–46]. While the binding energy of ZMC (−5.1 kcal/mol) is lower than that of the standard, such moderate affinities can still be biologically relevant, particularly when supported by additional stabilizing interactions and favorable cellular properties. Given ZMC's multifunctional profile and low cytotoxicity, the observed affinity remains within a range that warrants further investigation through quantitative and *in vivo* studies. Aberrant DNA methylation patterns are increasingly investigated as biomarkers for early detection and diseases stratification in T2D [47, 48]. Hence, compounds capable of modulating DNMT activity may offer valuable therapeutic potential in metabolic diseases.

Supporting this potential, preliminary live-cell imaging using methylation-sensitive fluorescent probes suggests that ZMC may influence DNA methylation dynamics, although quantitative validation remains necessary. While these early findings do not confirm epigenetic modulation, they indicate a possible role for ZMC in influencing methylation status.

Its confirmed effects on glycation, along with its emerging potential for epigenetic modulation, position ZMC as a strong candidate for further development in the treatment of T2D. Given that AG exhibits toxicity above 10 mM [49], ZMC's activity at lower concentrations, supported by previous studies showing minimal cytotoxicity at relevant doses [14, 50], further reinforces its therapeutic promise. Future work should include *in vivo* validation, mechanistic studies, and structural refinement to optimize ZMC's efficacy and safety in diabetic models.

Practical relevance. This study highlights the therapeutic potential of ZMC as a multi-target agent for T2D, addressing not only glycemic imbalance but also underlying mechanisms such as protein glycation and aberrant DNA methylation. Its *in vitro* efficacy supports its promise for future development as an orally administered adjunct or alternative therapy aimed at mitigating disease progression and complications. However, to ensure its safety and therapeutic efficacy, comprehensive preclinical toxicity studies are essential before advancing toward clinical application.

Research limitations. This study acknowledges several limitations that warrant further investigation. While the current findings provide compelling *in vitro* evidence of ZMC's therapeutic potential, further investigation using more physiologically relevant models such as advanced cellular systems and *in vivo* animal models of type 2 diabetes is essential to enhance translational value. Additional studies should assess the antioxidant capacity of ZMC through both cell-based and cell-free assays to clarify its role in mitigating oxidative stress. It is also recommended to evaluate its potential to enhance glucose uptake in C2C12 cells and its ability to mitigate reactive species generated under glucolipotoxicity conditions. Furthermore, elucidating the mechanism of action *in vivo*, particularly in relation to metabolic and epigenetic regulation, may provide deeper insights into its therapeutic relevance. Addressing these gaps will be critical in advancing ZMC from a promising candidate to a clinically meaningful intervention for type 2 diabetes.

Prospects for further research. Given the promising preliminary findings, several key directions are propose to advance the development and clinical relevance of ZMC in type 2 diabetes therapy. Future studies should evaluate its efficacy and safety in diabetic animal models to establish *in vivo* relevance. Investigating its impact on glucose uptake, insulin sensitivity, and oxidative stress in target cells such as skeletal muscle and adipocytes may clarify its metabolic role. Further exploration of its epigenetic effects, particularly on DNA methylation, could provide insight into its regulatory mechanisms. Structural optimization and formulation improvements may enhance bioavailability and therapeutic performance. Studies combining ZMC with existing antidiabetic agents could also reveal potential synergistic effects. These efforts will be essential to support ZMC's progression toward clinical application.

6. Conclusions

This study presents the first focused investigation of ZMC as a potential multi-target therapeutic for T2D. Beyond glycemic control, ZMC addresses two critical molecular drivers of T2D: protein glycation and aberrant DNA methylation. The successful synthesis and structural characterization of ZMC confirmed a stable, amorphous cyclic salt via bidentate coordination, supported by NMR, FT-IR, UV-Vis, elemental analysis, and PXRD data. Biological assays demonstrated that ZMC significantly inhibits AGE formation and protects protein structure in both glucose- and MGO-induced models.

Molecular docking and live-cell imaging suggest that ZMC may influence DNA methylation through interactions with DNMT1. However, no direct quantitative evidence, such as DNMT expression analysis, CpG profiling, or global methylation quantification, was obtained. Incorporating imaging-based quantification alongside molecular assays in future work would strengthen support for ZMC's proposed epigenetic effects.

Overall, ZMC shows promise as an integrative therapeutic candidate that combines antiglycation activity with potential epigenetic modulation. While these *in vitro* results are encouraging, validation in advanced cell systems and animal models is essential to assess its efficacy, safety, and metabolic impact. Future efforts should explore structural refinement, formulation strategies, and synergy with existing treatments. By bridging metabolic and epigenetic mechanisms, ZMC exemplifies a novel approach in diabetes therapy aimed at modifying disease progression at its molecular roots.

Conflict of interest

The authors declare no conflicts of interest, whether financial, personal, authorship-related, or otherwise, that could influence the research or its findings presented in this article.

Funding

This research was conducted with funding from Department of Science and Technology-Accelerated Science and Technology Human Resource Development Program (DOST-ASTHRDP). The primary author is also a recipient of the DOST-ASTHRDP Research Enrichment "Sandwich" Program which allowed him to perform experiments in Niigata University, Japan as a visiting researcher.

Data availability

Data will be made available on reasonable request

Use of artificial intelligence

The authors acknowledge the use of artificial intelligence tools for proofreading and structural refinement of the manuscript. All data generation, analysis, and interpretation were conducted and verified independently by the authors.

Acknowledgments

Department of Science and Technology-Accelerated Science and Technology Human Resource Development Program, Department of Science and Technology-Science Education Institute, Philippines, Premier Research Institute of Science and Mathematics, and Professor Yuichiro Hori of the Dynamic Chemical Life Science Laboratory (Kyushu University, Japan).

References

1. Sun, H., Saeedi, P., Karuranga, S., Pinkepank, M., Ogurtsova, K., Duncan, B. B. et al. (2022). IDF Diabetes Atlas: Global, regional and country-level diabetes prevalence estimates for 2021 and projections for 2045. Diabetes Research and Clinical Practice, 183, 109119. https://doi.org/10.1016/j.diabres.2021.109119

2. Five questions on the IDF Diabetes Atlas (2013). Diabetes Research and Clinical Practice, 102 (2), 147–148. https://doi.org/10.1016/j.diabres.2013.10.013

3. Zhou, B., Rayner, A. W., Gregg, E. W., Sheffer, K. E., Carrillo-Larco, R. M., Bennett, J. E. et al. (2024). Worldwide trends in diabetes prevalence and treatment from 1990 to 2022: a pooled analysis of 1108 population-representative studies with 141 million participants. The Lancet, 404 (10467), 2077–2093. https://doi.org/10.1016/s0140-6736(24)02317-1

4. Cando, L. F. T., Quebral, E. P. B., Ong, E. P., Catral, C. D. M., Relador, R. J. L., Velasco, A. J. D. et al. (2024). Current status of diabetes mellitus care and management in the Philippines. Diabetes & Metabolic Syndrome: Clinical Research & Reviews, 18 (2), 102951. https://doi.org/10.1016/j.dsx.2024.102951

5. Jiang, J., Zhao, C., Han, T., Shan, H., Cui, G., Li, S., Xie, Z., Wang, J. (2022). Advanced Glycation End Products, Bone Health, and Diabetes Mellitus. Experimental and Clinical Endocrinology & Diabetes, 130 (10), 671–677. https://doi.org/10.1055/a-1861-2388

6. Uceda, A. B., Mariño, L., Casasnovas, R., Adrover, M. (2024). An overview on glycation: molecular mechanisms, impact on proteins, pathogenesis, and inhibition. Biophysical Reviews, 16 (2), 189–218. https://doi.org/10.1007/s12551-024-01188-4

7. Ishrat, N., Khan, H., Patel, O. P. S., Mahdi, A. A., Mujeeb, F., Ahmad, S. (2021). Role of Glycation in Type 2 Diabetes Mellitus and Its Prevention through Nymphaea Species. BioMed Research International, 2021 (1). https://doi.org/10.1155/2021/7240046

8. Kim, M. (2019). DNA methylation: a cause and consequence of type 2 diabetes. Genomics & Informatics, 17 (4), e38. https://doi.org/10.5808/gi.2019.17.4.e38

9. Rönn, T., Ling, C. (2015). DNA Methylation as a Diagnostic and Therapeutic Target in the Battle Against Type 2 Diabetes. Epigenomics, 7 (3), 451–460. https://doi.org/10.2217/epi.15.7

10. Kaimala, S., Ansari, S. A., Emerald, B. S. (2023). DNA methylation in the pathogenesis of type 2 diabetes. Hormones and Epigenetics. Elsevier Inc., 147–169. https://doi.org/10.1016/bs.vh.2022.11.002

11. Chong, K., Chang, J. K., Chuang, L. (2024). Recent advances in the treatment of type 2 diabetes mellitus using new drug therapies. The Kaohsiung Journal of Medical Sciences, 40 (3), 212–220. https://doi.org/10.1002/kjm2.12800

12. Maanvizhi, S., Boppana, T., Krishnan, C., Arumugam, G. (2014). Metal complexes in the management of diabetes mellitus: A new therapeutic strategy. International Journal of Pharmacy and Pharmaceutical Science, 6, 40–44. Available at: https://journals.innovareacademics.in/index.php/ijpps/article/view/1778/10461

13. Matsukura, T., Tanaka, H. (2000). Applicability of Zinc Complex of L-Carnosine for Medical Use. Biochemistry, 65 (7), 817–823. Available at: https://pubmed.ncbi.nlm.nih.gov/10951100/

14. Tate, D. J., Newsome, D. A. (2006). A Novel Zinc Compound (Zinc Monocysteine) Enhances the Antioxidant Capacity of Human Retinal Pigment Epithelial Cells. Current Eye Research, 31 (7-8), 675–683. https://doi.org/10.1080/02713680600801024

15. Tate, D. J., Newsome, D. A. (2007). Preparation of a Zinc Monocysteine Compound. Synthetic Communications, 37 (6), 909–914. https://doi.org/10.1080/00397910601163612

16. Miroliaei, M., Khazaei, S., Moshkelgosha, S., Shirvani, M. (2011). Inhibitory effects of Lemon balm (Melissa officinalis, L.) extract on the formation of advanced glycation end products. Food Chemistry, 129 (2), 267–271. https://doi.org/10.1016/j.foodchem.2011.04.039

17. Ni, M., Song, X., Pan, J., Gong, D., Zhang, G. (2021). Vitexin Inhibits Protein Glycation through Structural Protection, Methylglyoxal Trapping, and Alteration of Glycation Site. Journal of Agricultural and Food Chemistry, 69 (8), 2462–2476. https://doi.org/10.1021/acs.jafc.0c08052

18. Hori, Y., Otomura, N., Nishida, A., Nishiura, M., Umeno, M., Suetake, I., Kikuchi, K. (2018). Synthetic-Molecule/Protein Hybrid Probe with Fluorogenic Switch for Live-Cell Imaging of DNA Methylation. Journal of the American Chemical Society, 140 (5), 1686–1690. https://doi.org/10.1021/jacs.7b09713

19. Brabha, M. J., Malbi, M. A. (2023). Synthesis, characterization and biological activity of zinc complexes of ethylenediamine and its derivatives. Chemical Physics Impact, 7, 100248. https://doi.org/10.1016/j.chphi.2023.100248

20. Campos, A. F. C., Reis, P. F., Neiva, J. V. C. M., Guerra, A. A. A. M., Kern, C., Silva, M. F. P. da et al. (2021). Reusable cysteine-ferrite-based magnetic nanopowders for removal of lead ions from water. Materials Research, 24 (5). https://doi.org/10.1590/1980-5373-mr-2021-0217

21. Soomro, R. A., Nafady, A., Sirajuddin, Memon, N., Sherazi, T. H., Kalwar, N. H. (2014). l-cysteine protected copper nanoparticles as colorimetric sensor for mercuric ions. Talanta, 130, 415–422. https://doi.org/10.1016/j.talanta.2014.07.023

22. Stark, F., Loderer, C., Petchey, M., Grogan, G., Ansorge-Schumacher, M. B. (2022). Advanced Insights into Catalytic and Structural Features of the Zinc-Dependent Alcohol Dehydrogenase from Thauera aromatica. ChemBioChem, 23 (15). https://doi.org/10.1002/cbic.202200149

23. Khan, M. M., Kalathil, S., Lee, J.-T., Cho, M.-H. (2012). Synthesis of Cysteine Capped Silver Nanoparticles by Electrochemically Active Biofilm and their Antibacterial Activities. Bulletin of the Korean Chemical Society, 33(8), 2592–2596. https://doi.org/10.5012/bkcs.2012.33.8.2592

24. Kieninger, M., Ventura, O. N. (2009). On the structure, infrared and Raman spectra of the 2:1 cysteine–Zn complex. Theoretical Chemistry Accounts, 125 (3-6), 279–291. https://doi.org/10.1007/s00214-009-0697-7

25. Guo, T., Xu, J., Fan, Z., Du, Y., Pan, Y., Xiao, H. et al. (2019). Preparation and characterization of cysteine-formaldehyde cross-linked complex for CO_2 capture. The Canadian Journal of Chemical Engineering, 97 (12), 3012–3024. https://doi.org/10.1002/cjce.23595

26. Zerner, M. C., Loew, G. H., Kirchner, R. F., Mueller-Westerhoff, U. T. (1980). An intermediate neglect of differential overlap technique for spectroscopy of transition-metal complexes. Ferrocene. Journal of the American Chemical Society, 102 (2), 589–599. https://doi.org/10.1021/ja00522a025

27. Han, J. (2010). Vibrational and Electronic Spectroscopic Characterizations of Amino Acid-Metal Complexes. Journal of the Korean Society for Applied Biological Chemistry, 53 (6), 821–825. https://doi.org/10.3839/jksabc.2010.124

28. Tripathi, I. P., Dwivedi, A., Mishra, M. K. (2019). Synthesis and Characterization of Some Zn (II) Complexes of L-Glutamic Acid and L-Aspartic Acid. International Journal of Advanced Scientific Research and Management, 5, 153–159. Available at: https://ijasrm.com/wp-content/uploads/2019/05/IJASRM_V4S4_1317_153_159.pdf

29. Trampuž, M., Žnidarič, M., Gallou, F., Časar, Z. (2022). Does the Red Shift in UV–Vis Spectra Really Provide a Sensing Option for Detection of N-Nitrosamines Using Metalloporphyrins? ACS Omega, 8 (1), 1154–1167. https://doi.org/10.1021/acsomega.2c06615

30. Timón, V., Maté, B., Herrero, V. J., Tanarro, I. (2021). Infrared spectra of amorphous and crystalline urea ices. Physical Chemistry Chemical Physics, 23 (39), 22344–22351. https://doi.org/10.1039/d1cp03503g

31. Kheshtzar, R., Berenjian, A., Taghizadeh, S.-M., Ghasemi, Y., Asad, A. G., Ebrahiminezhad, A. (2019). Optimization of reaction parameters for the green synthesis of zero valent iron nanoparticles using pine tree needles. Green Processing and Synthesis, 8 (1), 846–855. https://doi.org/10.1515/gps-2019-0055

32. Nazir, S., Anwar, J., Munawar, M. A., Best, S. P., Cheah, M. (2016). Transition Metal Complexes of S-Propyl- L -Cysteine. Journal of The Chemical Society of Pakistan, 38, 415–423. Available at: https://jcsp.org.pk/PublishedVersion/67f48146-16cf-4d24-bfe5-a74da9c85acfManuscript%20no%2006,%20Final%20Gally%20Proof%20of%2010829%20_Shahbaz%20Na.pdf

33. Yang, Y., Engkvist, O., Llinàs, A., Chen, H. (2012). Beyond Size, Ionization State, and Lipophilicity: Influence of Molecular Topology on Absorption, Distribution, Metabolism, Excretion, and Toxicity for Druglike Compounds. Journal of Medicinal Chemistry, 55 (8), 3667–3677. https://doi.org/10.1021/jm201548z

34. Lavilla, M. L., Lavilla, C. J. A., Burnea, F. K. B., Inutan, E. D. (2024). L-cysteine sequestering methyl glyoxal prevents protein glycation: a combined in vitro and in silico evaluation. Current Issues in Pharmacy and Medical Sciences, 37 (2), 114–120. https://doi.org/10.2478/cipms-2024-0019

35. Tarwadi, K. V., Agte, V. V., Kelkar, A. R. (2018). Influence of Selected Micronutrients on Glycation of Human Lens Proteins: Implications in Diabetic Cataract. Acta Scientific Ophthalmology, 1 (2), 4–10. Available at: https://actascientific.com/ASOP/pdf/ASOP-01-0009.pdf

36. Leyder, T., Mignon, J., Mottet, D., Michaux, C. (2022). Unveiling the Metal-Dependent Aggregation Properties of the C-terminal Region of Amyloidogenic Intrinsically Disordered Protein Isoforms DPF3b and DPF3a. International Journal of Molecular Sciences, 23 (23), 15291. https://doi.org/10.3390/ijms232315291

37. Tupe, R., Kulkarni, A., Adeshara, K., Sankhe, N., Shaikh, S., Dalal, S. et al. (2015). Zinc inhibits glycation induced structural, functional modifications in albumin and protects erythrocytes from glycated albumin toxicity. International Journal of Biological Macromolecules, 79, 601–610. https://doi.org/10.1016/j.ijbiomac.2015.05.028

38. Moulahoum, H., Ghorbanizamani, F., Timur, S., Zihnioglu, F. (2020). Zinc enhances carnosine inhibitory effect against structural and functional age-related protein alterations in an albumin glycoxidation model. BioMetals, 33 (6), 353–364. https://doi.org/10.1007/s10534-020-00254-0

39. Pace, N., Weerapana, E. (2014). Zinc-Binding Cysteines: Diverse Functions and Structural Motifs. Biomolecules, 4 (2), 419–434. https://doi.org/10.3390/biom4020419

40. Holendova, B., Plecita-Hlavata, L. (2023). Cysteine residues in signal transduction and its relevance in pancreatic beta cells. Frontiers in Endocrinology, 14. https://doi.org/10.3389/fendo.2023.1221520

41. Raciti, G. A., Desiderio, A., Longo, M., Leone, A., Zatterale, F., Prevenzano, I. et al. (2021). DNA Methylation and Type 2 Diabetes: Novel Biomarkers for Risk Assessment? International Journal of Molecular Sciences, 22 (21), 11652. https://doi.org/10.3390/ijms222111652

42. Cassandri, M., Smirnov, A., Novelli, F., Pitolli, C., Agostini, M., Malewicz, M. et al. (2017). Zinc-finger proteins in health and disease. Cell Death Discovery, 3 (1). https://doi.org/10.1038/cddiscovery.2017.71

43. Noronha, N. Y., Barato, M., Sae-Lee, C., Pinhel, M. A. de S., Watanabe, L. M., Pereira, V. A. B. et al. (2022). Novel Zinc-Related Differentially Methylated Regions in Leukocytes of Women With and Without Obesity. Frontiers in Nutrition, 9. https://doi.org/10.3389/fnut.2022.785281

44. Zhang, H.-H., Han, X., Wang, M., Hu, Q., Li, S., Wang, M., Hu, J. (2019). The Association between Genomic DNA Methylation and Diabetic Peripheral Neuropathy in Patients with Type 2 Diabetes Mellitus. Journal of Diabetes Research, 2019, 1–9. https://doi.org/10.1155/2019/2494057

45. Wang, X., Yang, W., Zhu, Y., Zhang, S., Jiang, M., Hu, J., Zhang, H.-H. (2022). Genomic DNA Methylation in Diabetic Chronic Complications in Patients With Type 2 Diabetes Mellitus. Frontiers in Endocrinology, 13. https://doi.org/10.3389/fendo.2022.896511

46. Hafez, S. M., Abou-Youssef, Hazem. E.-S., Awad, M. A.-K., Kamel, S. A., Youssef, R. N., Elshiekh, S. M. et al. (2021). Insulin-like growth factor binding protein 1 DNA methylation in type 2 diabetes. Egyptian Journal of Medical Human Genetics, 22 (1). https://doi.org/10.1186/s43042-021-00153-0

47. Willmer, T., Johnson, R., Louw, J., Pheiffer, C. (2018). Blood-Based DNA Methylation Biomarkers for Type 2 Diabetes: Potential for Clinical Applications. Frontiers in Endocrinology, 9. https://doi.org/10.3389/fendo.2018.00744

48. Cheng, Y., Gadd, D. A., Gieger, C., Monterrubio-Gómez, K., Zhang, Y., Berta, I. et al. (2023). Development and validation of DNA methylation scores in two European cohorts augment 10-year risk prediction of type 2 diabetes. Nature Aging, 3 (4), 450–458. https://doi.org/10.1038/s43587-023-00391-4

49. Ahmed, N. (2005). Advanced glycation endproducts – role in pathology of diabetic complications. Diabetes Research and Clinical Practice, 67 (1), 3–21. https://doi.org/10.1016/j.diabres.2004.09.004

50. Bulahan, G., Lavilla, C. (2025). Zinc-Cysteine Coupling Demonstrates Potent In Vitro Antioxidant Activity and Preserves Cell Viability Under Glucolipotoxicity-Induced Oxidative Stress. International Journal of Scientific Engineering and Science, 9 (5), 182–185. Available at: https://ijses.com/wp-content/uploads/2025/05/78-IJSES-V9N5.pdf

Received 16.06.2025
Received in revised form 17.07.2025
Accepted 22.08.2025
Published 30.08.2025

Godzelle Ogoc Bulahan*, Master of Science in Chemistry**,** Department of Chemistry**,** Mindanao State University – Iligan Institute of Technology, Bonifacio ave., Tibanga, Iligan City, Lanao del Norte, Philippines, 9200

Orlie B. Basalo, Master of Science in Chemistry, Department of Chemistry, Mindanao State University – Iligan Institute of Technology, Bonifacio ave., Tibanga, Iligan City, Lanao del Norte, Philippines, 9200

Hajime Iwamoto, PhD in Chemistry, Department of Chemistry, Niigata University, Ikarashi 2 Nochō, Nishi Ward, Niigata, Japan, 8050

Aaron L. Degamon, Master of Science in Chemistry, Department of Chemistry, Mindanao State University – Iligan Institute of Technology, Bonifacio ave., Tibanga, Iligan City, Lanao del Norte, Philippines, 9200

James V. Lavilla Jr., Master of Science in Chemistry, Department of Chemistry, Mindanao State University – Iligan Institute of Technology, Bonifacio ave., Tibanga, Iligan City, Lanao del Norte, Philippines, 9200

Richemae Grace R. Lebosada, PhD in Chemistry, Department of Chemistry, Mindanao State University – Iligan Institute of Technology, Bonifacio ave., Tibanga, Iligan City, Lanao del Norte, Philippines, 9200

Charlie A. Lavilla Jr., PhD in Biomedical Science**,** Department of Chemistry, Mindanao State University – Iligan Institute of Technology, Bonifacio ave., Tibanga, Iligan City, Lanao del Norte, Philippines, 9200

***Corresponding author:** Godzelle Ogoc Bulahan, e-mail: godzelle.bulahan*0505@g.msuiit.edu.ph